Proceedings of Meetings on Acoustics

JANUARY 29 2025

Using photographs to verify the nature of Mach wave radiation from a Falcon 9 rocket plume FREE

Grant W. Hart ; Kent L. Gee ; Eric G. Hintz; Nathan F. Carlston; Giovanna G. Nuccitelli; Trevor Mahlmann

Proc. Mtgs. Acoust. 54, 040012 (2024)
https://doi.org/10.1121/2.0002001

Volume 54 http://acousticalsociety.org/

Acoustics Week in Canada
Joint Meeting
186th Meeting of the Acoustical Society of America
and the Canadian Acoustical Association
Ottawa, Ontario, Canada
13-17 May 2024

Noise: Paper 1pNSa8

Using photographs to verify the nature of Mach wave radiation from a Falcon 9 rocket plume

Grant W. Hart, Kent L. Gee, Eric G. Hintz and Nathan F. Carlston
Department of Physics and Astronomy, Brigham Young University, Provo, UT, 84602; grant_hart@byu.edu; kentgee@byu.edu; hintz@byu.edu; nfc314@byu.edu

Giovanna G. Nuccitelli
Department of Mechanical Engineering, Brigham Young University, Provo, UT, 84602; gnucci17@byu.edu

Trevor Mahlmann
Professional Photographer, Cape Canaveral, FL 32920; trevor.mahlmann@gmail.com

At 7:30 AM on October 6, 2020 Space-X launched a Falcon-9 rocket from Kennedy Space Center. Photographer Trevor Mahlmann had positioned his camera in the location where the rocket would pass in front of the rising sun and took a series of images of that encounter. The high-intensity sound and shock waves originating in the plume are imaged by passing in front of the sun, particularly near the edge of the sun. This can be considered as a type of schlieren imaging system. The sound emitted from a supersonic rocket plume is thought to be due to Mach wave radiation. The images were processed to enhance the visibility of the propagating shock waves, and the propagation of those shock waves was traced back to the plume. This allowed the source location and emission direction of the sound to be determined. The measured shocks were found to be consistent with the predictions of Mach wave radiation from the plume, originating about 15-20 nozzle diameters down the plume, and radiating in a wide lobe peaking at about 70° from the plume direction. There are also indications that lower frequency waves are preferentially emitted at smaller angles relative to the plume.

Published by the Acoustical Society of America

 https://doi.org/10.1121/2.0002001

1. INTRODUCTION

Supersonic jets, and rockets in particular, produce significant noise. This noise can be measured and characterized by an array of microphones when the aircraft or rocket engine is static, but that is not typically how these machines are used. It is much more difficult to measure the noise produced when an aircraft or rocket is in flight, since the microphone array cannot be flown with it. Typically, microphones are placed on the ground and used to measure the aircraft sound radiation (Ward, 2024) as it passes by. This type of measurement is more difficult to understand than static measurements, because interpretation of the data requires both a knowledge of the vehicle trajectory and an assumption that the plume characteristics do not change with time. While this is frequently done, it is helpful to have another measurement technique that can corroborate the microphone-based measurements, without some of the same issues. This paper discusses a photographic measurement that allows a different visualization of the wave radiation during a Falcon 9 rocket launch.

Optical techniques, such as schlieren imagery (Weinstein, 1994) and background-oriented schlieren imagery (Heineck, 2020) have been used to image the large-scale shocks around supersonic aircraft in flight, but those techniques haven't been used to analyze the in-flight jet noise radiation. Shadowgraph and schlieren imaging have been used to image the wave radiation from supersonic jets in the laboratory, as demonstrated by e.g., Murray and Lyons (2016) and Seiner et al. (1994), but not for rockets in-flight.

In this paper we use photographs of a Falcon 9 passing in front of the Sun just after liftoff to image the radiated sound waves. The limb of the Sun acts as the knife-edge in a schlieren system, while the middle of the Sun acts more like a shadowgraph system. Analysis of these images allows verification of the properties of this radiation and shows it is consistent with Mach wave radiation.

2. PROPERTIES OF MACH WAVE RADIATION

Most of the sound from a supersonic jet is thought to come in the form of Mach wave radiation originating downstream in the plume from the jet nozzle (see Lubert et al., 2022, and references therein for a description of the properties of Mach wave radiation). Figure 1 illustrates the structure of the plume of a rocket. As the gas emerges from the nozzle on the left side of the picture, it is in a state of laminar flow. As it interacts with the ambient atmosphere, the outer edges become turbulent. The region where the flow is still laminar is called the potential core. The region where the flow is still supersonic, but turbulent, is called the supersonic core, as shown in Figure 1. Surrounding the supersonic core is the mixing layer, which is turbulent gas, with subsonic speeds.

Mach wave radiation is not isotropic; it has a preferred direction given by

$$\theta = \cos^{-1}\left(\frac{1}{M_c}\right),$$

where M_c is the convective Mach number of the jet. This preferred direction is the center of a band that is about 30° wide. High frequencies are radiated mostly from the region of the plume near the nozzle, where the supersonic core is thin, and the eddies must be small enough to fit. These radiate preferentially at large angles. Longer wavelength, and therefore lower frequency waves, come from the larger eddies located farther downstream from the nozzle, where the mixing layer is thicker. They are radiated preferentially at smaller angles relative to the plume. Given the geometry of the source, it is clear that the source acts more like a line source than a point source. For the specific case here, a Falcon 9 has an Oertel convective Mach number (Greska et al. 2008) of 2.81, giving an expected peak at 69.1° relative to the plume (Mathews et al., 2021). This is in good agreement with another Mach number relation recently obtained by Gee *et al*. (2024), where the convective Mach number is the square root of the fully expanded jet acoustic Mach number. Using the parameters of Mathews et al. (2021), $M_c = 2.98$ and $\theta = 70.4°$.

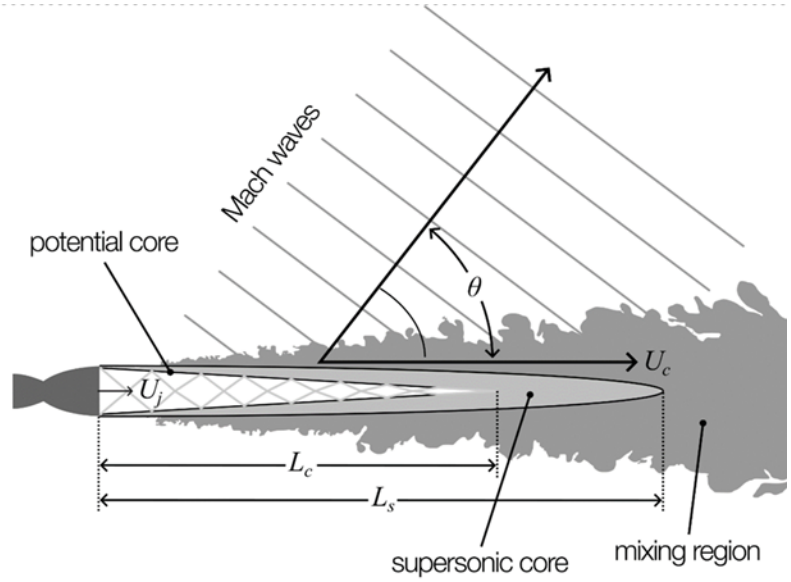

Figure 1. Diagram of a supersonic jet (Gee et al., 2024). The potential core is a region of nearly laminar flow coming from the nozzle. Shock cells, shown by the crossing lines in the potential core, and caused by wave reflection from the edges can be seen. Surrounding that is the supersonic core, where the flow is still supersonic, but not fully laminar. Around that is the subsonic mixing region. Mach waves are generated at the interface of the supersonic core and the mixing region. Larger eddies downstream tend to make the lower-frequency waves that propagate at smaller angles relative to the direction of the plume.

3. OCTOBER 6, 2020 FALCON-9 LAUNCH

On October 6, 2020, SpaceX launched a set of 60 Starlink satellites from Cape Canaveral, Florida a few minutes after sunrise, as illustrated by the photograph in Figure 2. As can be seen in the figure, the Sun was about 2° above the horizon at the time of launch.

Because of the early morning timing of the launch, launch photographer Trevor Mahlmann had carefully arranged the position of his camera so the rocket would pass in front of the Sun from his vantage point. Figure 3 shows three frames from the sequence of pictures that he took. Part (A) of the figure shows the time when the rocket just touches the bottom of the Sun, part (B) shows when the rocket was about halfway across, and part (c) shows a frame when the rocket has completely transited the Sun and the plume is still visible over the face of the Sun. The camera was set on an automatic trigger, and it took pictures at as fast a rate as it could. In total there were 24 frames in the sequence of pictures. These photographs provided an opportunity to image the wave field around the rocket plume and measure some of its characteristics.

Figure 2. Launch of a Falcon-9 rocket on October 6, 2020, a few minutes after sunrise. As can be seen from this picture, the sun was about 2° above the horizon at the time of launch. Photo credit: SpaceX (license CC BY-NC 2.0)

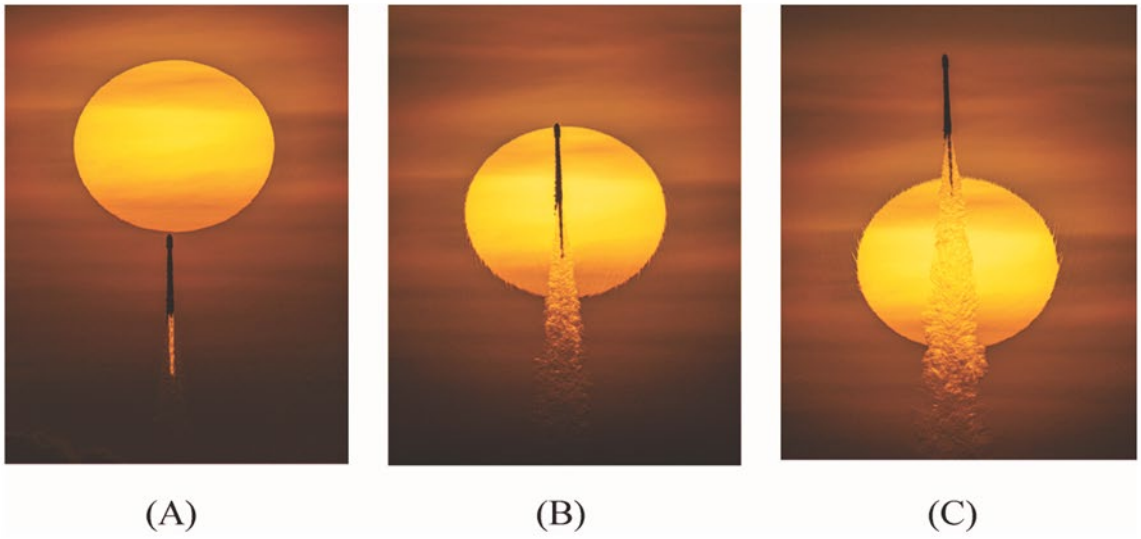

Figure 3. Several frames from the series of photographs taken by Trevor Mahlmann during the launch. Frame (A) is taken just as the rocket touches the Sun, (B) is when the base is halfway across, and (C) is when the rocket has passed beyond the Sun. The slightly oblate shape of the Sun is caused by atmospheric refraction due to the closeness to the horizon.

4. INTERESTING PHYSICS FROM THE PICTURES

As can be seen in Figure 4, the bright illumination of the Sun highlights several interesting physical phenomena. In part (A) of the figure, the potential core of the supersonic plume is clearly illuminated. The shock

cells are visible as the dark and light pattern in the potential core. Looking carefully at the edge of the Sun in part (B), shock waves can be seen as bright lines on both sides of the Sun. The presence of these lines implies that we should be able to measure some characteristics of the sound waves from these pictures and gain a holistic view of the sound field around the rocket, rather than the point measurements provided by a microphone. However, the images need some manipulation to allow the sound field to be more clearly imaged.

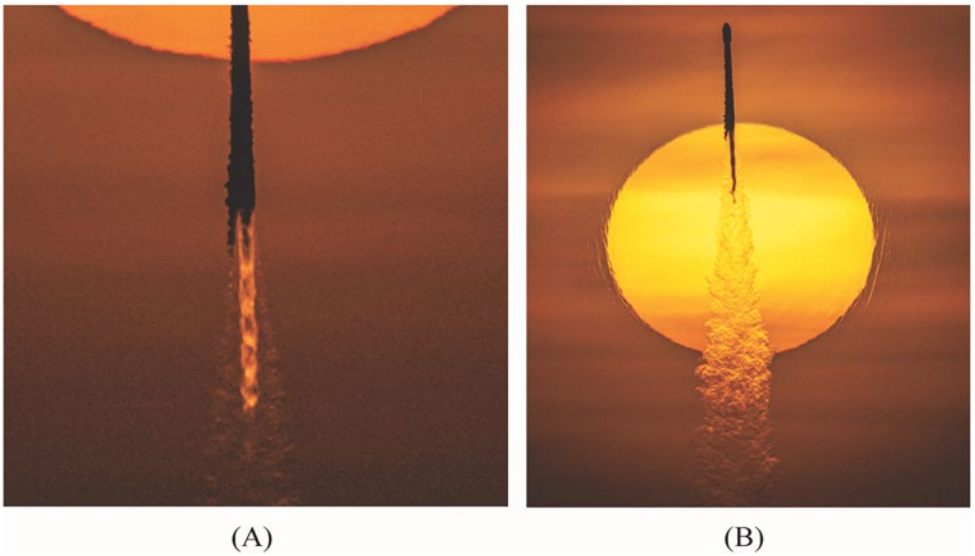

Figure 4. In part (A) the potential core is well illuminated and the shock cells in the core are clearly visible. In part (B) shock waves are also visible near the edge of the Sun.

5. IMAGE PROCESSING TECHNIQUES

We used the MaxIm DL software (published by Diffraction Limited, referenced below) to align each frame with the original frame which contained the Sun with the rocket barely off of the Sun's image. The Sun frame was then subtracted from each subsequent frame to reduce the impact of the bright Sun on waves visible in the images. This removes, or at least greatly reduces, anything that has not changed between the two images and enhances the visibility of the waves. The result of this part of the process is shown in part (A) of Figure 5. The rocket in the original image can be seen as a light version of the rocket at the bottom of the Sun, while the later image of the rocket is darker and is positioned such that is just leaving the Sun. The main plume comes from the center of the rocket and a cloud of cryogenic vapor can be seen on the left side of the rocket.

The next step in making the waves clearer was to manipulate the color curves of the image using GIMP (Gnu Image Manipulation Program) to increase the contrast and brightness of the waves at the expense of any other detail in the picture. The result of that process is shown in part (B) of Figure 5. The waves both inside and outside the image of the Sun are much more visible than before.

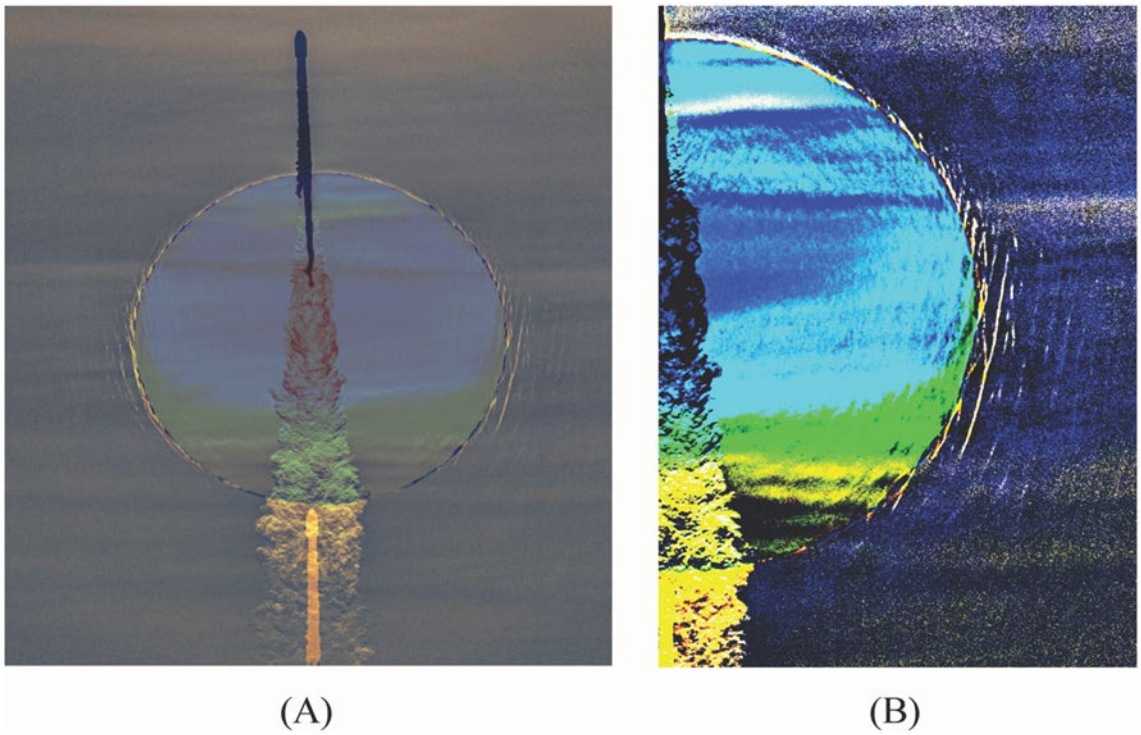

Figure 5. Processed images. To obtain part (A) the images were aligned to put the Sun in the same place in each frame. The first image was then subtracted from all the other images, removing anything that didn't change between images, therefore highlighting the waves. To obtain part (B) the color curves were changed to enhance the contrast of the waves with the background.

6. FINDING THE SOURCE OF THE WAVES

Verification that the sound produced has the characteristics of Mach wave radiation requires that the sound waves be traced back to their source, and that the position of the rocket at the time of emission be found. This requires a determination of the vehicle trajectory across the Sun, as well as the spacing of the frames in time. The metadata on the pictures only specified the time down to the minute, and so all the frames showed the same time.

Several factors needed to be known to find the frame times. The rocket is known to be 70 m tall, which gave a physical scale for the images. We could measure the top and bottom positions of the rocket in each frame, using the bottom of the Sun as our origin. Knowing that the center of the Sun was at approximately 2.1° above the horizon (see Figure 1), the height of the rocket above the ground could be determined.

Both the velocity and altitude of the rocket as a function of time were extracted from the telemetry on the livestream video of the launch. A least-squares fit of the position and velocity of the rocket to the measurements on the pictures allowed the determination of the spacing of the frames in time relative to each other. An equal time-spacing of the frames wasn't consistent with the pictures; the position errors from assuming an equal spacing were much bigger than allowed by the uncertainty in the measurement. Since the motion of the rocket is known to be smooth, this allowed the determination of the actual times of the frames.

Figure 6 shows the results of this calculation. The line is the trajectory of the center of the rocket across the Sun and the dots indicate the position of the rocket's nozzle at the time of each frame. The frames were found to be approximately 1/5 of a second apart, with considerable jitter, caused by the different processing times necessary in the camera between frames.

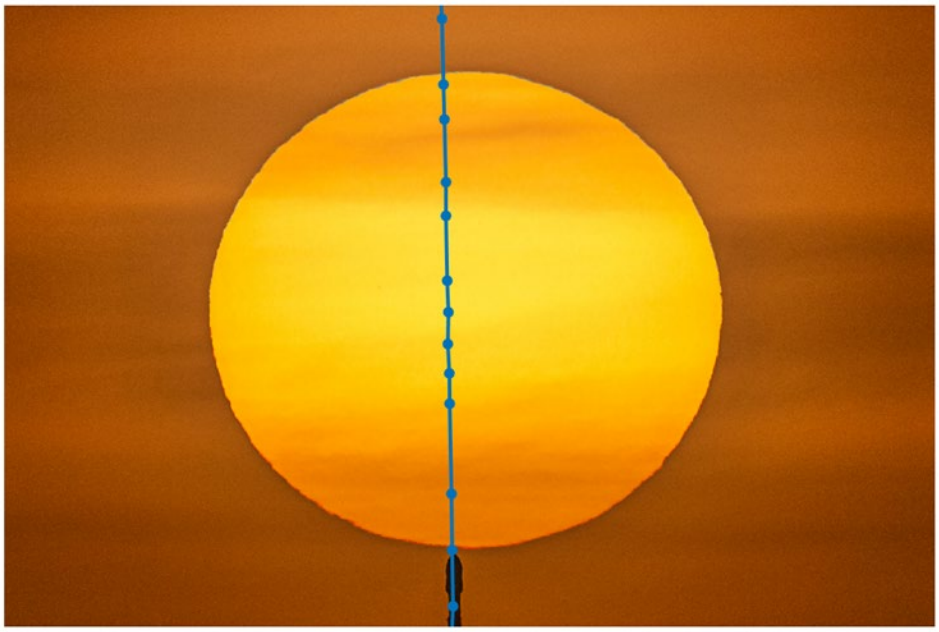

Figure 6. Trajectory of the bottom of the rocket across the Sun. The blue line is the rocket's path across the Sun. The blue dots show the location of the bottom of the rocket in each frame of the sequence. The frames are not equally spaced in time.

Figure 7 shows the steps in the process to determine the emission position of a given shock wave relative to the nozzle. Part (A) shows the selection of the desired shock wave. It is indicated on the figure as a red line segment on the right-hand-side of the figure, slightly above the middle of the picture. A line is then drawn perpendicular to the line segment, over to the trajectory line. Using the length of this line, which is shown by the orange line in part (B) of the figure, it is possible to calculate the time the shock took to propagate from the source to its current position. The National Weather Service reported that the temperature at Kennedy Space Center was 75°F at the time of the launch, giving a sound speed of 345 m/s. The rocket was only a few hundred meters above the pad as it crossed the Sun, so the surface temperature should be a good approximation to the temperature around the outside of the plume. It is likely that this propagation time is an overestimate, since the sound source is located at the edge of the plume, rather than at its center, but it is difficult to correct properly.

Knowing the propagation time, the position of the rocket at the time of emission can easily be determined from the trajectory. The distance from the bottom of the rocket to the point of intersection of the trajectory with the propagation ray is then calculated. This is shown in part (C) of the figure. The box at the top of the figure shows the calculated position of the rocket at emission time. The yellow double-ended arrow indicates the distance from the rocket nozzle to the emission point.

The two important parameters are now determined. As is traditional in jet theory, the distance is scaled by the effective nozzle diameter, which is the diameter of an equivalent nozzle that has the same cross-sectional area as all the actual nozzles combined. For a Falcon-9 rocket, that is $D_{\text{eff}} = \sqrt{9}\, D = 3D$, where D is the diameter of a single engine. This is 2.76 m. In the rocket literature emission angles are measured relative to the direction of the plume, so the angle of propagation in Figure 7 is the angle measured from the trajectory to the orange line, which in this case is about 78°.

Part (D) of the figure shows most of the wave locations that were used in the analysis of this particular frame. The analysis was then repeated for all of the frames that had visible waves.

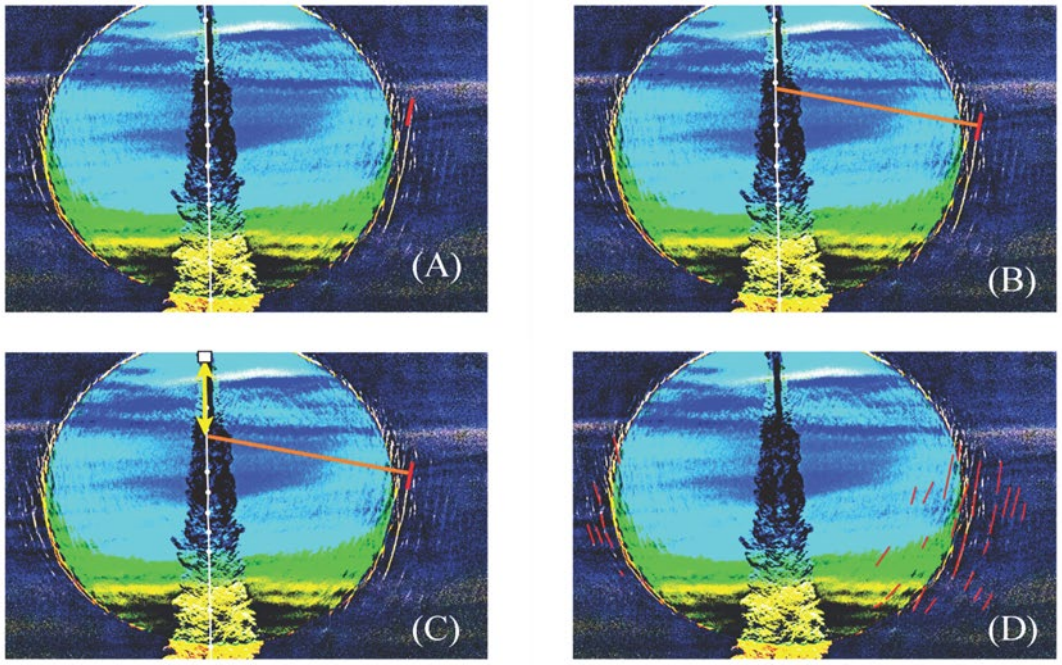

Figure 7. Procedure to find the wave source. A wavefront is selected, as shown by the red line in part (A) of the figure. The line perpendicular to that wavefront is drawn back to the rocket's trajectory line. This is shown as the orange line in part (B). From the length of that line the propagation time is determined and the position of the rocket's nozzle at the emission time is found. This is illustrated by the white box at the top of part (C) of the figure. The distance (shown as a yellow arrow in part (C)) is then found. It is then scaled by the effective nozzle diameter, as is usual in the supersonic jet literature. The red lines in part (D) show the many wavefront locations used in analyzing this frame.

One other type of analysis that is done on each frame is to determine the frequency of the waves observed. Since these are likely shock waves and not linear sinusoidal wavefronts, it is unclear how close the spacing of the shocks is to the wavelength of the underlying waves. This analysis assumes that every high-amplitude peak produces a shock wave. To determine the frequency of a set of wavefronts, a line of known length is drawn perpendicular to the waves in question. The number of wavefronts intersected is counted, and the length of the line is divided by the number of wavefronts. This gives an estimate of the wavelength, which is converted to frequency using the speed of sound. This is done for many sets of waves on a given frame, and they are all averaged to give the average frequency of that frame. This is a very rough measure of frequency, since many waves, particularly when the frequency gets low, don't have more than one wavefront to measure between. This limits the ability of this measure to get a spectrum of the sound. Also, there is also no guarantee that all the wavefronts crossing a particular line have the same source. This process as outlined seems to work on average, though, for the higher frequency range where multiple wavefronts can be seen.

7. RESULTS

Each frame of the sequence highlights a different part of the plume, since only those waves that pass near to the edge of the Sun get highlighted by sharp contrast of the edge. So early frames, when the bottom of the rocket has barely entered the Sun, tend to show the waves that originate close to the nozzle. These waves propagate at large angles relative to the plume, near 90°. When the rocket's bottom is near the top of the Sun, the sound source is near the middle of the Sun and waves that are produced in all parts of the plume can be seen. When the rocket is well above the Sun, only those waves that originate far down the plume can be seen. This is illustrated in

Figure 8. The plot shows the distance down the plume of the sound source versus the propagation angle. The distance down the plume is shown from the top of the figure toward the bottom, aligning with the orientation of a rocket. Consider the rocket nozzle to be at the top and the plume pointing downward. Angles are measured relative to the plume flow direction.

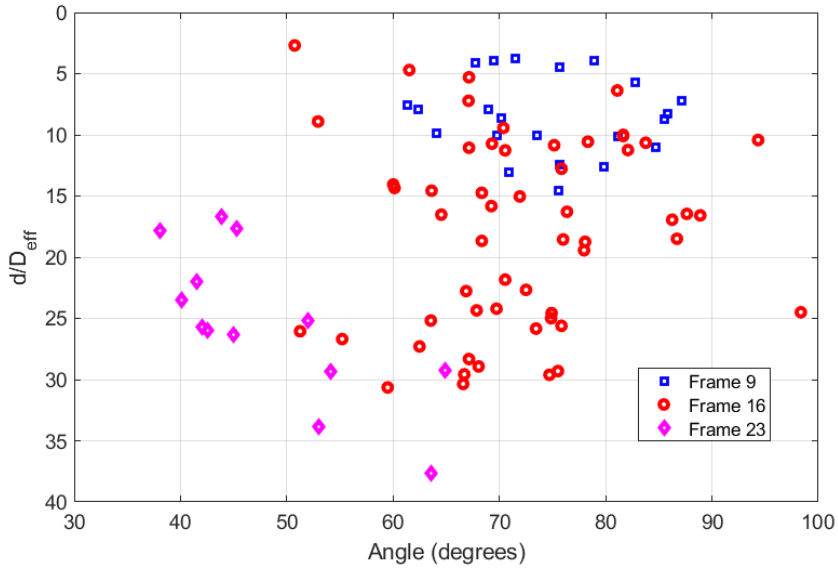

Figure 8. Sound radiation angle versus the apparent position of the sound source. The rocket nozzle is located at the top of the figure, with the distance from the nozzle increasing downward. Because different parts of the plume are located in front of the Sun in different frames, each frame highlights a different part of the plume. The blue squares are from Frame 9, where the plume is starting to move in front of the Sun. This emphasizes the small-downstream-distance, high-angle waves. By Frame 16 (red circles) most of the plume is over the Sun and waves with many source positions and angles are produced. When Frame 23 is reached, only the distant part of the plume is still highlighted. Therefore, the data show mostly small angles and large distances.

In Frame 9 the nozzle of the rocket is slightly more than one quarter of the way across the Sun. The points measured in Frame 9 are shown as blue squares, and they tend to be clustered in the upper-right had corner of the figure, indicating waves produced close to the nozzle and at large angles to the plume. Frame 16 has the rocket's nozzle about 90% of the way across the Sun, so most of the sound-source region is in front of the Sun and waves are seen at many different source positions and angles. These points are shown in Figure 8 as red circles. By Frame 23, the rocket's nozzles are well beyond the top of the Sun, at about 2/3 of its diameter above the top. Only sound produced far down the plume is visible in this frame, and it is mostly at small angles. These waves are shown as magenta diamonds in the figure.

Figure 9 shows a histogram of all the angles and downstream distance for all the frames put together. The histogram peaks between 15 and 20 nozzle diameters downstream and at an angle of about 70 degrees. Both are in line with measurements made from the ground and expectations of Mach wave radiation. This histogram does not necessarily represent the actual distribution of sound energy, because of potential bias in the selection of wavefronts calculated and not all wavefronts are of equal energy density. Also of note is the angular width of the distribution. The full-width-half-maximum of the peak is about 30°, which agrees qualitatively with the acoustically measured distribution of sound (Lubert et al. 2022).

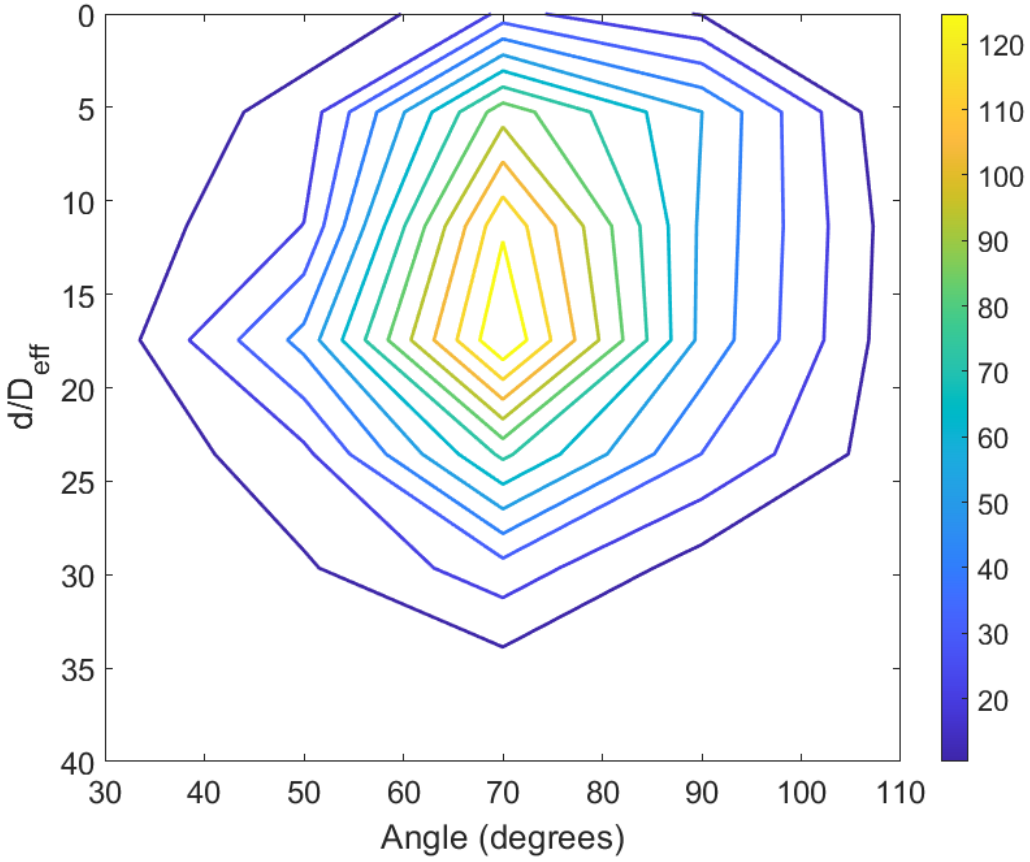

Figure 9. A histogram of the number of waves accumulated from all frames. Again, the rocket nozzle is at the top and the distance increases downward. The peak occurs between 15 and 20 nozzle diameters downstream and at an angle of about 70°. Note that the width of the distribution is about 30°.

Another way of presenting the data is shown in Figure 10. Since each frame tends to highlight a different part of the plume, we can get a picture of the sound production by plotting the average of d/D_{eff} vs. the average angle for each frame. The rocket is again located at the top of the plot and distance down the plume goes downward on the plot. The early frames are in the upper-right-hand corner of the plot and as frame number increases the points move downward and to the left. The fact that frame 9 shows an average angle greater than 90° probably indicates that many of the waves measured in that frame are not Mach waves, but rather are other waves that propagate in a more isotropic manner. The waves measured in Frame 9 are measured very close to the source, so it may actually be in the near field of the rocket's sound source. This has been seen previously in acoustic intensity measurements of a GEM-60 solid rocket booster, where sound a short distance down the plume was actually seen radiating at near 90° or larger angles (Gee et al., 2016).

As mentioned at the end of Section 6, it is possible to also calculate the average frequency of waves in a particular frame. Figure 11 has the average frequency for a given frame plotted versus the average angle of emission of the waves in that frame. While somewhat noisy, as expected for the quantities involved, it is evident that lower frequencies are emitted at smaller angles and the average frequency goes up as the distance from the nozzle decreases. Taken together with Figure 10, this shows that lower frequencies tend to be produced farther down the plume, as expected (Lubert et al., 2022, Gee et al., 2016).

A parameter that is often used to describe the frequency of jet noise is the Strouhal number, $S = \frac{D_e f}{U_e}$, where D_e is the effective nozzle diameter and U_e is the exit velocity of the nozzle. Using the parameters of the Falcon 9, the upper limit on Figure 11 corresponds to a Strouhal number of 0.08 and the bottom limit corresponds to a

Strouhal number of 0.027. These are both above the expected Strouhal number of the spectral peak of the Falcon 9 (Mathews et al., 2021), showing the insensitivity of this photographic method to the lowest frequencies.

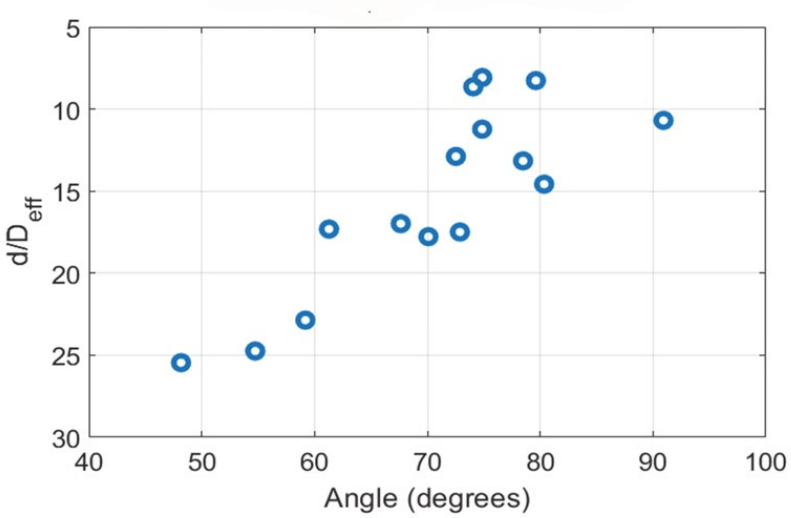

Figure 10. Distance down the plume vs. angle, averaged over each frame. The y-axis is again plotted with the rocket at the top and distance down the plume plotted downward on the axis. Early frames are in the upper-right hand corner of the plot, and they move down to the lower left as frame number increases.

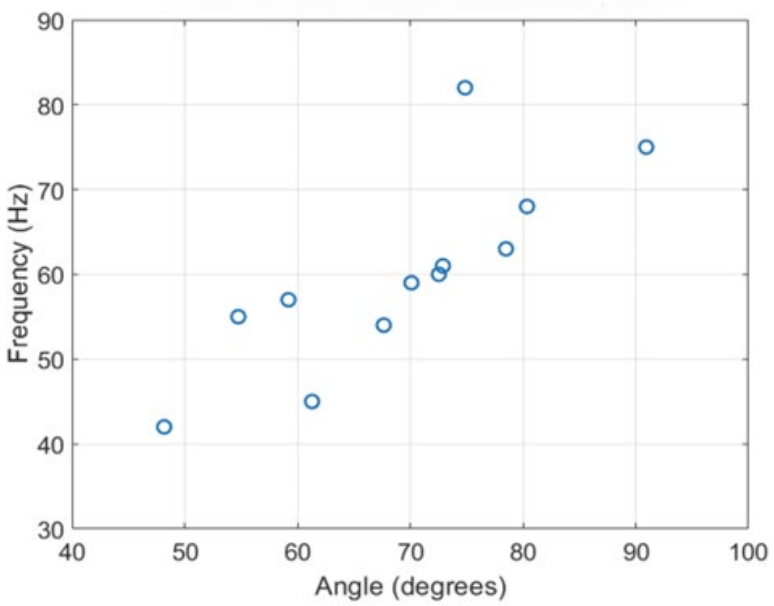

Figure 11. Average frequency vs. angle, averaged over individual frames. While somewhat noisy, this plot shows that on average lower frequencies propagate at smaller angles.

8. CONCLUSION

These results are all consistent with the source of the observed waves being due to Mach wave radiation. The criteria we are comparing to are:

1. The peak in the radiation goes in the direction of $\theta = \cos^{-1}\left(\frac{1}{M_c}\right)$, where M_c is the convective Mach number of the rocket. For a Falcon-9 rocket, M_c is calculated to be approximately 2.8, giving a peak directivity angle of close to 70°, consistent with what we see in Figure 9.
2. The width of the radiation emission is expected to be relatively wide. Again, this is consistent with Figure 9.
3. The peak position of the radiation source is expected to be about 17-18 nozzle diameters down the plume, consistent with Figure 9.
4. Sound radiated farther up the plume tends to go at larger angles, as shown in Figure 10. This combined with the fact that lower frequencies tend to be produced at lower angles (Figure 11) means that on average lower frequencies are produced farther down the plume. This is consistent with the fact that the mixing region is larger farther down the plume (see Figure 1), which allows larger turbulent eddies to form, producing longer wavelength and therefore lower frequency waves.
5. One limitation of this analysis is that it cannot measure the frequencies of low frequency waves, so getting a measure of the spectrum of a rocket, which typically peaks a very low frequencies, is not possible this way.

The analysis of photographs such as these allows a complementary view of the sound radiation from a rocket compared to microphone measurements. The field of view of a photograph allows us to measure the entire range of the radiation field around the plume, as opposed to merely a set of points where microphones are located. It also allows us to make these measurements in the free field as the rocket is in flight, something that would be extremely challenging to do with microphones.

REFERENCES

Diffraction Limited, of Ottawa, Canada, is the maker of Cyanogen Imaging® MaxIm DL™ software. Cyanogen Imaging is a Registered Trademark, and MaxIm DL is a Trademark of Diffraction Limited. (2024)

Kent L. Gee, Eric B. Whiting, Tracianne B. Neilsen, Michael M. James, Alexandria R. Salton, "Development of a Near-field Intensity Measurement Capability for Static Rocket Firings", Trans. JSASS Aerosp. Tech. Jpn. 14, Po_2_9–Po_2_15 (2016).

Kent L. Gee, Tyce W. Olaveson, and Logan T. Mathews, "Convective Mach Number and Full-Scale Supersonic Jet Noise Directivity", AIAA J. (2024)

B. Greska, A. Krothapalli, W. C. Horne, and N. Burnside, "A Near-Field Study of High Temperature Supersonic Jets," in Proceedings of the 14th AIAA/CEAS Aeroacoustics Conference (29th AIAA Aeroacoustics Conference), Vancouver, BC (May 5–7, 2008), AIAA 2008-3026.

James T. Heineck, Daniel W. Banks, Nathanial T. Smith, Edward T. Schairer, Paul S. Bean, and Troy Robillos. "Background-oriented schlieren imaging of supersonic aircraft in flight." *AIAA Journal* **59**, 11 (2021) .

Caroline P. Lubert, Kent L. Gee, and Seiji Tsutsumi, "Supersonic jet noise from launch vehicles: 50 years since NASA SP-8072", J. Acoust. Soc. Am. **151**, 752 (2022).

Logan T. Mathews, Kent L. Gee, and Grant W. Hart, "Characterization of Falcon 9 launch vehicle noise from far-field measurements", J. Acoust. Soc. Am. **150**, 620 (2021).

Nathan E. Murray and Gregory W. Lyons (2016), "On the convection velocity of source events related to supersonic jet crackle", J. Fluid Mech. **793**, 477 (2016).

J. M. Seiner, T. Bhat, and M. Pointon, "Mach wave emission from a high-temperature supersonic jets." AIAA J. 32 (12), 2345–2350 (1994).

Jacob A. Ward, "Nonlinear modeling of in-flight noise from high-performance military aircraft", Master's Thesis, Department of Physics and Astronomy, Brigham Young University (2024).

L. M. Weinstein, "An Optical Technique for Examining Aircraft Shock Wave Structures in Flight," NASA CP 3279, 1 (1994).